Journal of Neuroscience Methods 293 (2018) 289–298

Contents lists available at ScienceDirect

Journal of Neuroscience Methods

journal homepage: www.elsevier.com/locate/jneumeth

Research Paper

Online detection of amplitude modulation of motor-related EEG desynchronization using a lock-in amplifier: Comparison with a fast Fourier transform, a continuous wavelet transform, and an autoregressive algorithm

Kenji Kato[a,b,1,2], Kensho Takahashi[a,1], Nobuaki Mizuguchi[a,c], Junichi Ushiba[a,d,*]

[a] Faculty of Science and Technology, Keio University, 3-14-1 Hiyoshi, Kohoku-ku, Yokohama, Kanagawa, 223-8522, Japan
[b] Department of Rehabilitation Medicine, Keio University School of Medicine, 35 Shinanomachi, Shinjuku, Tokyo, 160-8582, Japan
[c] The Japan Society for the Promotion of Science, 5-3-1 Kojimachi, Chiyoda-ku, Tokyo, 102-0083, Japan
[d] Keio Institute of Pure and Applied Sciences (KiPAS), Keio University, 3-14-1 Hiyoshi, Kohoku-ku, Yokohama, Kanagawa, 223-8522, Japan

HIGHLIGHTS

- We applied a lock-in amplifier (LIA) algorithm for online electroencephalogram (EEG) analyses.
- The LIA detected EEG motor-imagery-related amplitude modulation.
- We evaluated the detection delay, accuracy, and stability of the LIA.
- The LIA improved all three indices compared with an existing online algorithm.

ARTICLE INFO

Article history:
Received 14 April 2017
Received in revised form 16 October 2017
Accepted 17 October 2017

Keywords:
Brain–computer interface (BCI)
Online neurofeedback
Electroencephalogram (EEG)
Lock-in amplifier (LIA)
Event-related desynchronization (ERD)
Sensorimotor cortex (SM1)
Motor imagery

ABSTRACT

Background: Neurofeedback of event-related desynchronization (ERD) in electroencephalograms (EEG) of the sensorimotor cortex (SM1) using a brain–computer interface (BCI) paradigm is a powerful tool to promote motor recovery from post-stroke hemiplegia. However, the feedback delay attenuates the degree of motor learning and neural plasticity.
New method: The present study aimed to shorten the delay time to estimate amplitude modulation of the motor-imagery-related alpha and beta SM1-ERD using a lock-in amplifier (LIA) algorithm. The delay time was evaluated by calculating the value of the maximal correlation coefficient (MCC) between the time-series trace of ERDs extracted by the online LIA algorithm and those identified by an offline algorithm with the Hilbert transform (HT).
Results: The MCC and delay values used to estimate the ERDs calculated by the LIA were 0.89 ± 0.032 and 200 ± 9.49 ms, respectively.
Comparison with Existing Method(s): The delay time and MCC values were significantly improved compared with those calculated by the conventional fast Fourier transformation (FFT), continuous Wavelet transformation (CWT), and autoregressive (AR) algorithms. Moreover, the coefficients of variance of the delay time and MCC values across trials were significantly lower in the LIA compared with the FFT, CWT, and AR algorithms.
Conclusions: These results indicate that the LIA improved the detection delay, accuracy, and stability for estimating amplitude modulation of motor-related SM1-ERD. This would be beneficial for BCI paradigms to facilitate neurorehabilitation in patients with motor deficits.

* Corresponding author at: Department of Biosciences and Informatics, Faculty of Science and Technology, Keio University, 3-14-1 Hiyoshi, Kouhoku-ku, Yokohama, Kanagawa 223-8522, Japan.
E-mail address: ushiba@brain.bio.keio.ac.jp (J. Ushiba).
[1] These authors contributed equally to this work.
[2] Present address: Center of Assistive Robotics and Rehabilitation for Longevity and Good Health, National Center for Geriatrics and Gerontology, 7-430, Morioka-cho, Obu, Aichi 474-8511, Japan.

https://doi.org/10.1016/j.jneumeth.2017.10.015
0165-0270/

1. Introduction

Many studies have demonstrated that an electroencephalogram (EEG)-based brain–computer interface (BCI) can facilitate functional motor recovery in patients with hemiplegia due to stroke (Daly and Wolpaw 2008; Daly et al., 2009; Broetz et al., 2010; Prasad et al., 2010; Wang et al., 2010; Ang et al., 2011; Caria et al., 2011; Shindo et al., 2011; Ramos-Murguialday et al., 2013; Mukaino et al., 2014; Ang et al., 2015; Ono et al., 2015). This type of BCI often detects modulation of EEG oscillations (i.e., event-related desynchronization; ERD) over the primary sensorimotor area (SM1) induced by motor imagery; then, a visual display, motor-driven orthosis, or neuromuscular electrical stimulation provides visual/sensory feedback. Neurofeedback of SM1-ERD helps patients learn to activate cortical neurons, as SM1-ERD in the alpha (8–13 Hz) and beta bands (15–30 Hz) reflects cortical and spinal neuron excitability (Hummel et al., 2002) and gamma-aminobutyric acid (GABA)ergic intracortical disinhibition of cortical neurons (Takemi et al., 2013).

To detect modulation of motor-imagery-related SM1-ERD, some research groups have employed spectral analysis with fast Fourier transformation (FFT) (Shindo et al., 2011; Krusienski et al., 2012; Wang et al., 2013; Ge et al., 2014; Mukaino et al., 2014; Takemi et al., 2013, 2015; Ono et al., 2013, 2014, 2015), continuous wavelet transformation (CWT) (Cvetkovic et al., 2008; Al-Fahoum and Al-Fraihat, 2014), or an autoregressive (AR) model (Gunduz et al., 2012; Wang et al., 2012; Ramos-Murguialday et al., 2013). However, these algorithms are associated with a feedback delay >500 ms because of the time window needed to reliably estimate the ERD. Since visual feedback delay attenuates the effects of motor adaptation process (Kitazawa et al., 1995; Tanaka et al., 2011; Honda et al., 2012; Schween and Hegele, 2017), a BCI system with a short feedback delay would allow for more control of BCI in patients with motor deficits.

To reduce the feedback delay, the present study developed a novel online algorithm to estimate the amplitude modulation of motor-imagery-related SM1-ERD using a lock-in amplifier (LIA). The LIA is a very narrow, tunable filter that delivers amplitude and phase information of the carrier wave at a specific frequency in real time. Since the LIA enables reliable and point-by-point calculations of signal components with simple multiplication and filtering algorithms, it might be possible to develop a more reliable online algorithm to estimate the amplitude modulation of ERD with less delay.

To evaluate the performance of the online LIA algorithm, we calculated correlation coefficients between the ERD obtained by the online LIA algorithm and that obtained by the offline Hilbert transform (HT); the HT generates an ideal trace of amplitude modulation without a time delay. The accuracy and delay of the performance were determined by the value of the maximal correlation coefficient (MCC) and the time lag where MCC was detected. Last, we compared the accuracy and delay calculated by the online LIA algorithm with those calculated by the conventional online FFT, CWT, and AR algorithms in various time windows and overlap parameters.

2. Methods

2.1. Participants

Twenty healthy male participants (average age, 24.2 ± 2.9 years) were included in this study. All participants were right-handed, had no medical or psychological disorders (according to self-reports), and had normal or corrected-to-normal vision. All participants received a detailed explanation of the experimental procedures before the experiment, and written informed consent was obtained from all participants. The experimental protocol used in the study was in accordance with the Declaration of Helsinki and was approved by the ethics committee of Keio University.

2.2. Experimental paradigm

Each participant sat in a comfortable armchair and was asked to perform motor imagery (i.e., isometric right wrist extension). A 20-inch computer monitor was placed 60–90 cm in front of them. Each trial started with a presentation of the word “Rest” at the center of the monitor. After 5 s, the presented word changed to “Image,” which remained for 5 s. After the motor imagery phase, the screen was black for 3 s. In this phase, the participants were allowed to move freely. After that, the monitor showed the word “Rest,” and the next trial started. All participants completed 25 trials.

2.3. EEG recordings

EEG was recorded over the whole scalp using 128-channels (Geodesic Sensor Nets, Oregon, USA). The impedance of each electrode was maintained at less than 40 kΩ throughout the experiment (Ferree et al., 2001). The EEG signals were amplified and recorded at a sampling rate of 1000 Hz after DC remove, band-pass (3–70 Hz), and notch (50 Hz) filters with a fourth-order Butterworth filter by the Geodesic EEG System (Electrical Geodesics Incorporated [EGI], Oregon, USA). The EEG signals were spatially filtered with a large Laplacian filter, which subtracted the average of the next-nearest-neighbor electrodes (6 channels and 4 cm from the C3 electrode). Then, band-pass (3–70 Hz) and notch (50 Hz) filters with a fourth-order Butterworth filter were applied again via offline processing to segregate the entire brain-derived signal from noise. Last, a software-based calculation with FFT, CWT, AR, and LIA algorithms that emulated real-time processing was tested in this study (MATLAB 2016a; MathWorks, Massachusetts, USA).

2.4. Emulation of online ERD calculation with FFT

First, we used an FFT algorithm as the conventional method to estimate the alpha and beta amplitude modulations (Shindo et al., 2011; Mukaino et al., 2014; Takemi et al., 2013, 2015; Ono et al., 2013, 2015). To calculate the ERD, EEG data were processed using the following 4 steps: (1) segmentation of 0.1-, 0.25-, 0.5-, or 1-s time windows with 0, 50, 90, or 99% overlap; (2) power spectrum density (PSD) calculation by FFT algorithm with a Hanning window; (3) determination of a frequency of interest (FOI), which showed the most significant ERD over the alpha and/or beta bands by visual inspection; and (4) ERD transformation (Takemi et al., 2013). A reference time from 3 to 5 s in each resting phase was used to estimate ERD.

2.5. Emulation of online ERD calculation with CWT

Second, a CWT algorithm with a complex Morlet function was used as the conventional method to estimate the alpha and beta amplitude modulations (Cvetkovic et al., 2008; Al-Fahoum and Al-Fraihat, 2014). According to the commonly used parameter ranges of time windows and overlaps, ERD was calculated after the following 4 steps: (1) segmentation of 0.1-, 0.25-, 0.5-, or 1 s time windows with 0, 50, 90, or 99% overlap; (2) PSD calculation by the CWT algorithm with a complex Morlet function; (3) determination of an FOI, which showed the most significant ERD over the alpha and/or beta bands by visual inspection; and (4) ERD transformation. A reference time from 3 to 5 s in each resting phase was used to estimate ERD.

2.6. Emulation of online ERD calculation with AR model

Third, an AR model fitted with the Burg method was used as the conventional algorithm to estimate the alpha and beta amplitude modulations (Burg, 1972; Bos et al., 2002; Gunduz et al., 2012; Wang et al., 2012; Ramos-Murguialday et al., 2013; Al-Fahoum and Al-Fraihat, 2014). According to the commonly used parameter ranges of the model, order, time window, and overlapping, ERD was calculated after the following 4 steps: (1) segmentation of 0.1-, 0.25-, 0.5-, or 1 s time windows with 0, 50, 90, or 99% overlap; (2) PSD estimation by an AR algorithm of the 25th order with the Burg method; (3) determination of an FOI, which showed the most significant ERD over the alpha and/or beta bands by visual inspection; and (4) ERD transformation. A reference time from 3 to 5 s in each resting phase was used to estimate ERD.

2.7. Emulation of online ERD calculation with LIA

The block diagram in Fig. 1 illustrates the LIA processing flow used in the present study. Lock-in measurements can extract signal amplitude in a defined frequency band around the reference frequency using point-by-point multiplication and integration of the non-filtered input with a reference trigonometric basis signal. The proposed LIA process first extracts the component at the FOI (f_r) with a narrow band-pass filter ($f_r \pm 1$ Hz) since noise components nearby FOI are contaminated in EEG; this differs from general assumptions made when using the original LIA algorithm. Then, the filtered input signal was split and multiplied separately with a reference signal and a $\pi/2$ phase-shifted copy of it (i.e., those from a reference trigonometric basis signal) to calculate the amplitude of the extracted signal.

Assuming that the input signal is defined as $A(t)\sin(2\pi f_r t + \phi) + n(t)$, where A is the amplitude of the signal, ϕ is the phase, and $n(t)$ is the noise component, and the reference signal is defined as $\sin(2\pi f_r t)$ and $\cos(2\pi f_r t)$, the outputs after s

$$\left\{A(t)\sin(2\pi f_r t + \phi) + n(t)\right\} * \sin(2\pi f_r t) = \left(\frac{A(t)}{2}\right) [\cos(2\pi f_r t + \phi) - \cos\phi] + n(t)\sin(2\pi f_r t) \quad (1)$$

$$\left\{A(t)\sin(2\pi f_r t + \phi) + n(t)\right\} * \cos(2\pi f_r t) = \left(\frac{A(t)}{2}\right) [\sin(2\pi f_r t + \phi) - \sin\phi] + n(t)\cos(2\pi f_r t) \quad (2)$$

If the output is segmented into T s (=$1/f_r$) and then smoothed, the AC signal and noise components are removed and the DC signal remains. In this case, the smoothed output is represented as follows.

$$X_{out} = \left(\frac{A(t)}{2}\right)\cos(\phi) \quad (3)$$

$$Y_{out} = \left(\frac{A(t)}{2}\right)\sin(\phi) \quad (4)$$

Then, the amplitude and phase were obtained after performing polar conversion.

$$R_{out} = \sqrt{{X_{out}}^2 + {Y_{out}}^2} = \frac{A(t)}{2} \quad (5)$$

$$\theta_{out} = \tan^{-1}\frac{X_{out}}{Y_{out}} = \phi \quad (6)$$

It is again noted that the present study applied a narrow band-pass filter ($f_r \pm 1$ Hz) before multiplication of the input with the reference signal, while the original LIA diagram typically applies a low-pass filter after multiplication. In this study, we used a second-order Butterworth band-pass filter with a 1 s time window, and segmentation of T s (=1/FOI) EEG data with a 99% overlap time window. Last, the amplitude modulations calculated by the LIA were transformed into ERD traces (Takemi et al., 2013). FOI was determined as the frequency at which the most significant ERD followed by the motor imagery task was observed in the FFT spectral analysis over the alpha and/or beta band. A reference time of 3–5 s in each resting phase was used to estimate the ERD. A pilot experiment in five healthy participants was performed to confirm the relationship between the band-pass filtering order, delay time, and detection accuracy (Supplementary Table 1), suggesting that the detection accuracy in the second-order filtering was the highest. Therefore, the present study applied the second band-pass filter to the online LIA algorithm.

2.8. Extraction of ideal ERD trace

To compare the accuracy and delay of the ERD amplitude modulation by the online LIA and conventional algorithms (i.e., FFT, CWT, and AR), an ideal amplitude modulation signal with no time delay at the FOI was calculated by the HT algorithm (Claerbout, 1985; Feldman, 2011). To calculate the ERD, EEG data were processed in the following 3 steps: (1) application of a second-order alpha band-pass filter (the central frequency was the FOI) on both sides of the signal; (2) a full-wave rectification followed by the HT; and (3) transformation of the envelope to the ERD (Takemi et al., 2013). A reference time of 3–5 s was used to estimate the ERD.

2.9. Correlation analysis

To estimate the accuracy of and the delay necessary to detect alpha/beta amplitude modulation by the online algorithms (i.e., FFT, CWT, AR, or LIA), we performed a correlation analysis on the waveforms of ERDs obtained by the online FFT, CWT, AR, or LIA algorithm and the offline HT algorithm. The ERDs estimated by the HT algorithm were shifted with a time window of 1000 ms in every sample (1 ms), from 0 to 1500 ms, and the correlation coefficient was calculated at every time and trial. Then, the values of the correlation coefficients were averaged across all trials in each participant. We defined the delay as the time point that showed the maximal correlation coefficient (MCC) between the online FFT, CWT, AR, or LIA algorithm and the offline HT algorithm.

2.10. Statistics

We calculated the average MCC values and delay time, and their coefficients of variance (CV) across all participants. A paired t-test was performed on the mean values of the MCC obtained by the online conventional (i.e., FFT, CWT, or AR) and proposed (LIA) algorithms after Fisher's z transformation. A paired t-test was also performed between the values of the coefficients of variance obtained by the online conventional (i.e., FFT, CWT, or AR) and proposed LIA algorithms. Similarly, a paired t-test was performed between the average values of the delay obtained by the online conventional (i.e., FFT, CWT, or AR) and proposed LIA algorithms. A Wilcoxon signed-rank test was performed between the coefficients of variance obtained by the online conventional (i.e., FFT, CWT, or AR) and proposed LIA algorithms after performing an F-test. Data values are expressed as mean ± 1 standard deviation. Statistical significance was set at a level of $p < 0.05$.

3. Results

A representative example of an average time–frequency map recorded over the SM1 during the motor imagery task is shown in Fig. 2**A**, illustrating a clear motor-imagery-related ERD over the alpha frequency range. The alpha ERD topography identified from

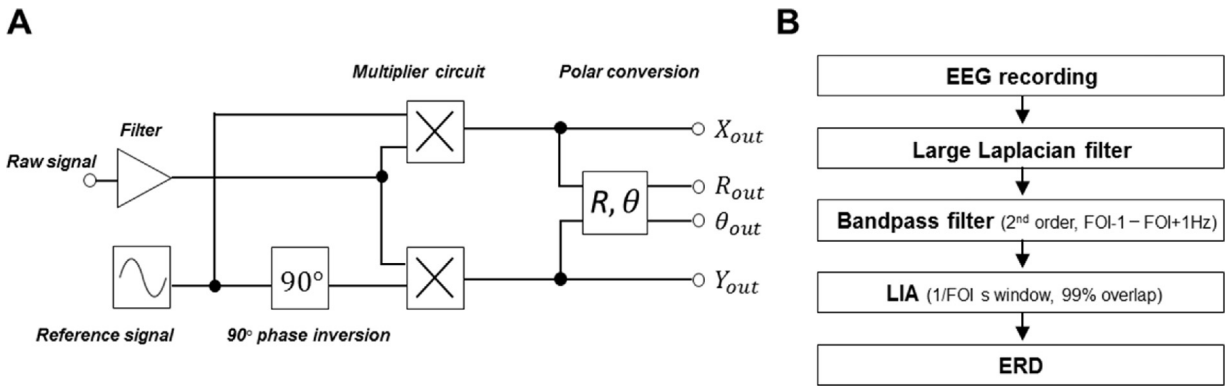

Fig. 1. Block diagram of the lock-in amplifier (LIA) (A) and flow chart for calculating event-related desynchronizations (ERDs) with the online LIA algorithm (B).

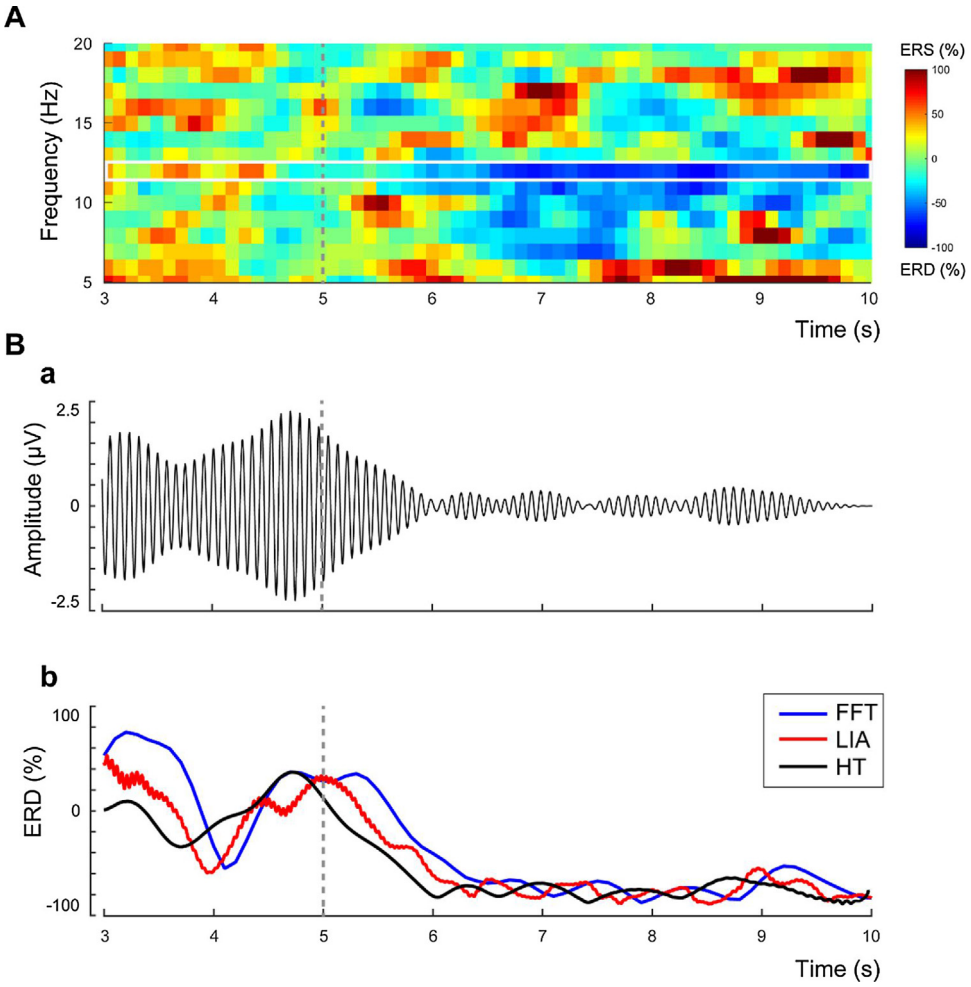

Fig. 2. Raw data of the ERD trends extracted by the online LIA algorithm.
A. Time–frequency map of ERDs in the alpha band collected over the primary sensorimotor cortex (SM1) of a representative participant from the calibration session. The vertical gray dotted line represents the onset of the motor imagery task. The amplitude of the oscillation over 12 Hz clearly decreased following the motor imagery task, illustrated by the white rectangle. **B**. The filtered oscillatory activity at the frequency of interest (FOI; i.e., 12 Hz) is shown (**a**). The ERDs calculated by the online LIA (red line), online fast Fourier transformation (FFT) with a 1 s window and 90% overlap (blue line), and the offline Hilbert transform (HT) algorithms (black line) are shown (**b**). The vertical gray dotted line represents the onset of the motor imagery task (For interpretation of the references to colour in this figure legend, the reader is referred to the web version of this article.).

128-channel EEG data showed further that the alpha ERD was focused on the sensorimotor areas (Supplementary Fig. 1). The FOI for the LIA calculation was determined to be at 12 Hz, the most significant alpha SM1-ERD observed during the motor imagery task (illustrated in the white rectangle in Fig. 2**A**). Therefore, the amplitude modulation of 12 Hz oscillations recorded over the SM1 was calculated by the online LIA algorithm (red line in Fig. 2**Bb**). It was noted that the waveforms of the ERDs calculated by the online LIA algorithm could track the ideal 12 Hz oscillatory envelope calculated by the offline HT algorithm (black line in Fig. 2**Bb**). In addition, it was clear that the LIA envelope decreased more quickly following the motor imagery task than did that calculated by the conven-

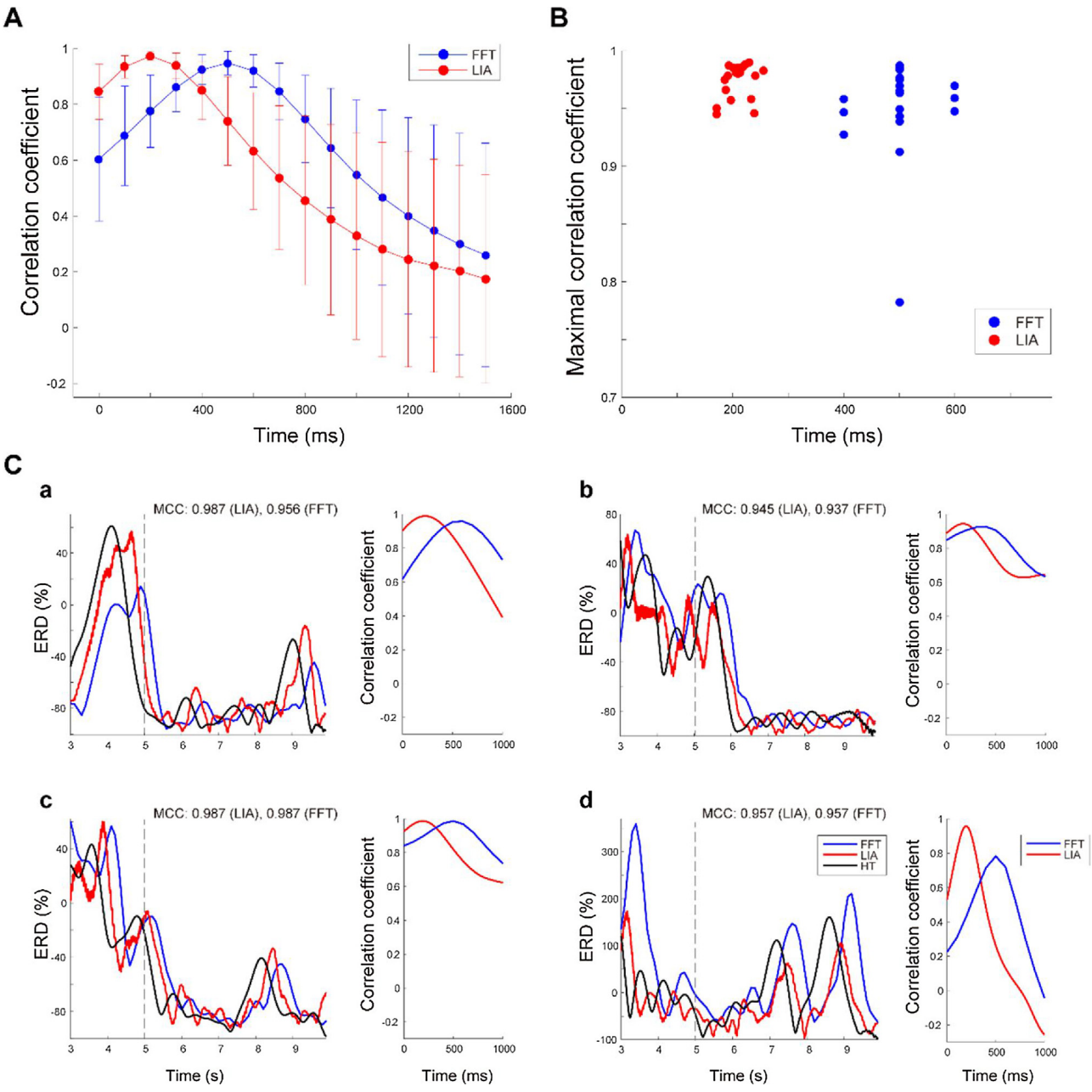

Fig. 3. Representative example of correlation coefficients between amplitude modulation of ERDs calculated by the online LIA or FFT algorithm and the offline HT algorithm. **A.** The average correlation coefficient at each time point between ERD traces calculated by the online LIA (red line) or FFT (blue line) with a 1-s window and 90% overlap and ideal ERD traces calculated by the HT across all trials is shown in a representative participant. The error bars represent the standard deviation. **B**. Maximal correlation coefficient (MCCs) calculated by the online LIA (red dots) and FFT (blue dots) algorithms are plotted from all trials of a representative participant. **C**. Representative examples of the time-series trace of ERD calculated by the online LIA (red line), online FFT (blue line), and HT (black line, assumed as an ideal ERD trace) algorithms are shown in the left panel. The correlation coefficients from the LIA (red line) and FFT (blue line) are plotted in the right panel. Representative trials showing the highest (**a**) and lowest (**b**) MCC values in the online LIA algorithm and the highest (**c**) and lowest (**d**) MCC values in the online FFT algorithm are plotted (For interpretation of the references to colour in this figure legend, the reader is referred to the web version of this article.).

tional online FFT algorithm with a 1 s window and 90% overlap (blue line in Fig. 2**Bb**), suggesting that the online LIA algorithm could more instantaneously detect the alpha oscillation desynchronization at the FOI following the motor imagery task than could the FFT algorithm.

To assess the estimation accuracy and delay time, mean correlation coefficients between ERD traces were calculated across 25 trials using the online FFT with a 1-s window and 90% overlap or LIA algorithm. Data from a representative participant are shown in Fig. 3**A**; the MCCs from each trial are plotted in Fig. 3**B**. The average delay was 210 ± 16.4 ms and 478 ± 64.7 ms obtained by the online LIA and FFT, respectively. The averaged MCC values obtained by the online LIA and FFT were 0.86 ± 0.062 and 0.80 ± 0.10, respectively. The online LIA results showed a shorter delay and greater ERD estimation accuracy than did the online FFT algorithm. Trials representing the highest and lowest MCC values in the online LIA and FFT (Fig. 3**C**) were used to examine how MCC variability occurred across trials. We found that the envelopes calculated by the LIA could track the ideal envelope (calculated by the HT) more instantaneously than those by the FFT in trials with the highest and lowest MCC values.

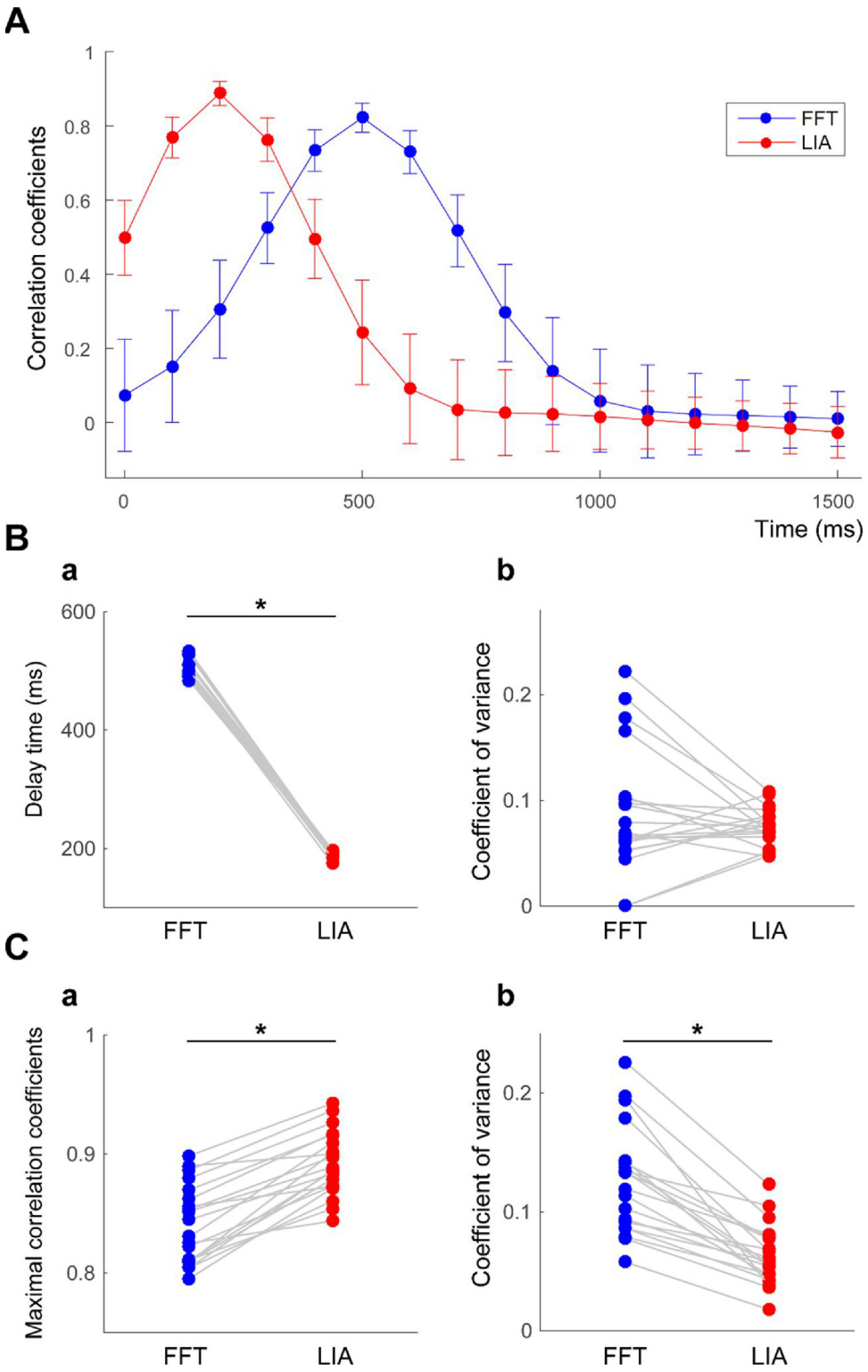

Fig. 4. Detection accuracy and time delay of the alpha ERD calculated by the online LIA and FFT algorithms averaged across participants.
A. The average correlation coefficient at each time point between the online LIA (red line) or FFT (blue line) with a 1-s window and 90% overlap and offline HT across all participants is shown. The error bars represent the standard deviation. **B**. Comparison of the time delay values that showed MCCs calculated by the LIA (red dot) and FFT (blue dot) in all participants (**a**). Comparison of the time delay coefficients of variance calculated by the LIA (red dot) and FFT (blue dot) in all participants (**b**). **C**. Comparison of the values of the MCC calculated by the LIA (red dot) and FFT (blue dot) in all participants (**a**). Comparison of the coefficients of variance of the MCC calculated by the LIA (red dot) and FFT (blue dot) in all participants (**b**)(For interpretation of the references to colour in this figure legend, the reader is referred to the web version of this article.).

The correlation coefficients obtained from the online LIA and FFT algorithms with a 1 s window and 90% overlap were averaged across 20 healthy participants (Fig. 4**A**). The average delays estimated by the online LIA algorithm were significantly shorter than those estimated by the online FFT algorithm (LIA: 200 ± 9.49 ms; FFT: 503 ± 18 ms; $p < 1.0^{*}10^{-25}$; Fig. 4**Ba**), suggesting that the online LIA algorithm could estimate faster than could the online FFT algorithm. The MCC values calculated by the LIA were signifi-

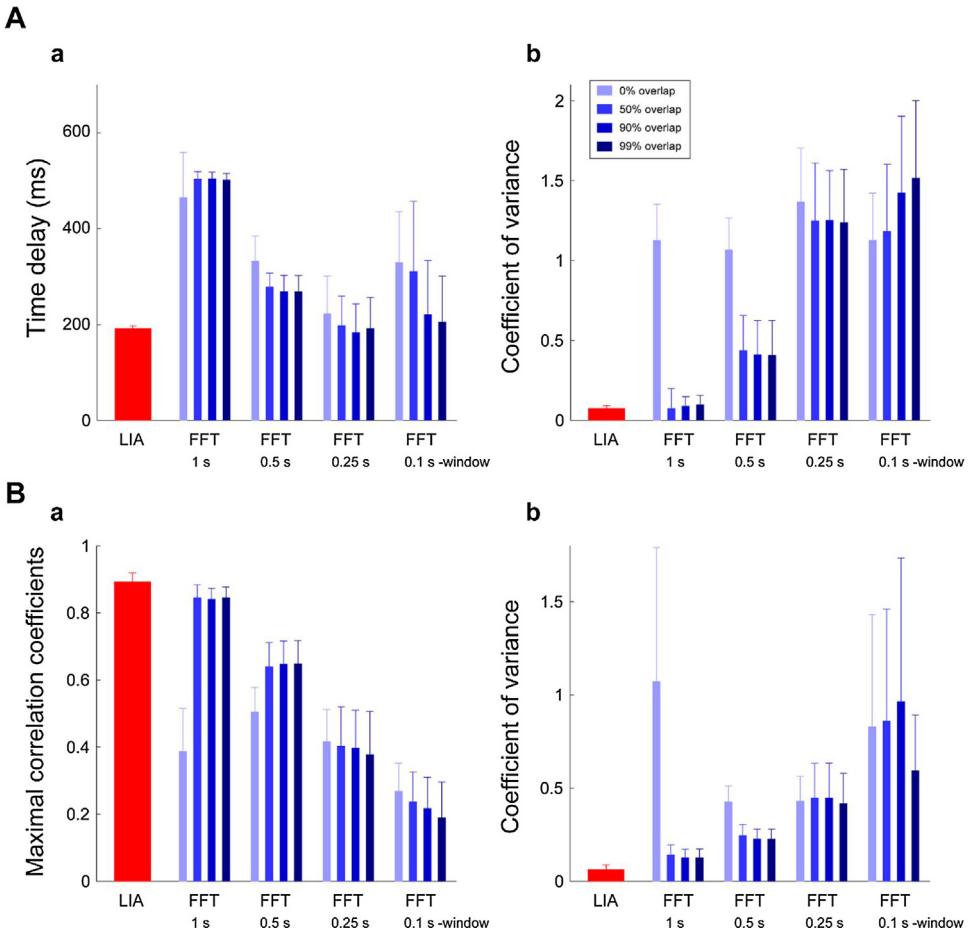

Fig. 5. Comparison of the ERD accuracy and time delay calculated by the online LIA and FFT algorithms in all time windows and overlaps.
A. The average time delay calculated by the online LIA (red bar) and FFT (blue bars) with 1-, 0.5-, 0.25-, and 0.1-s time windows and 0, 50, 90, and 99% overlaps (**a**). The average time delay coefficient of variance calculated by the online LIA (redbar) and FFT (blue bars) with 1-, 0.5-, 0.25-, and 0.1 s time windows and 0, 50, 90, and 99% overlaps (**b**). The error bars represent the standard deviation. **B**. The average MCC calculated by the online LIA (red bar) and FFT (blue bars) with 1-, 0.5-, 0.25-, and 0.1-s time windows and 0, 50, 90, and 99% overlaps (**a**). The average coefficient of variance of the MCC calculated by the online LIA (redbar) and FFT (blue bars) with 1-, 0.5-, 0.25-, and 0.1-s time windows and the 0, 50, 90, and 99% overlaps (**b**). The error bars represent the standard deviation (For interpretation of the references to colour in this figure legend, the reader is referred to the web version of this article.).

cantly greater than those calculated by FFT (LIA: 0.89 ± 0.032; FFT: 0.83 ± 0.038; $p < 1.0^{*}10^{-10}$; Fig. 4**Ca**), suggesting that the online LIA algorithm could more accurately estimate the envelopes of the motor-imagery-related SM1 desynchronizations than could the online FFT algorithm. The coefficient of variance of the MCC was significantly lower in the online LIA than in the FFT algorithm (LIA: 0.0617 ± 0.0215; FFT: 0.1300 ± 0.0338; $p < 1.0 \times 10^{-9}$; Fig. 4**Bb**), suggesting that the detection accuracy of the online LIA algorithm was more stable than that of the online FFT algorithm. In addition, we confirmed that 6 out of 20 participants displayed motor-imagery-related SM1-ERDs over both the alpha and beta frequency bands (Supplementary Fig. 2**A**). Thus, LIA was adapted to beta oscillations in addition to alpha oscillations. As a result, the LIA improved the time delay, MCC, and their CVs to detect the beta amplitude modulations, as compared with the FFT algorithm with a 1-s window and 90% overlap (Supplementary Fig. 2**B**).

Next, we investigated whether the online LIA algorithm could maintain the accuracy and delay advantages over various online FFT algorithm parameters, such as time window and overlap (Fig. 5). We demonstrated that alpha ERD estimation by the online LIA algorithm was more accurate ($p < 10^{-10}$; Fig. 5**Ba**) and stable ($p < 0.01$; Fig. 5**Ab** and 5**bb**) than those estimated by the online FFT algorithm in all time windows (i.e., 0.1, 0.25, 0.5, and 1 s) and overlaps (i.e., 0, 50, 90, and 99%). The time delays calculated by the LIA were significantly shorter than that in the FFT in almost all time windows and overlaps ($p < 0.05$; Fig. 5**Aa**). However, the 0.1- and 0.25 s time windows with 90% and 99% overlaps were comparable (Fig. 5**Aa**). Overall, these results suggested robust advantages of the LIA algorithm in terms of the accuracy, delay, and stability regardless of the online FFT algorithm parameters. As for the beta ERD estimation, the improvements of the LIA algorithm in terms of the delay, accuracy, and stability were similarly maintained irrespective of these parameters (see *p*-values in Supplementary Table 2).

The accuracy, delay, and stability to detect the alpha and beta amplitude modulations by the LIA algorithm were evaluated and compared with the other commonly used conventional algorithms of the CWT (Fig. 6) and AR (Fig. 7). As was the case for the FFT, the average time delays estimated by the LIA were significantly shorter than those by the CWT in the 1- and 0.5-s time windows ($p < 10^{-5}$; Fig. 6**Aa**) and AR algorithms in all time windows and overlaps ($p < 10^{-3}$; Fig. 7**Aa**); however, the time delay in the LIA was sometimes longer than that in the CWT in the 0.1- and 0.25-s time windows ($p < 0.01$; Fig. 6**Aa**). On the other hand, the MCC values calculated by the LIA were significantly greater than those calculated by the CWT ($p < 10^{-3}$; Fig. 6**Cb**) and AR algorithms ($p < 10^{-5}$; Fig. 7**Cb**) for every parameter (also see the beta estimation results in Supplementary Table 2). In addition, the coefficient of variance of the time delay and MCCs was significantly lower in

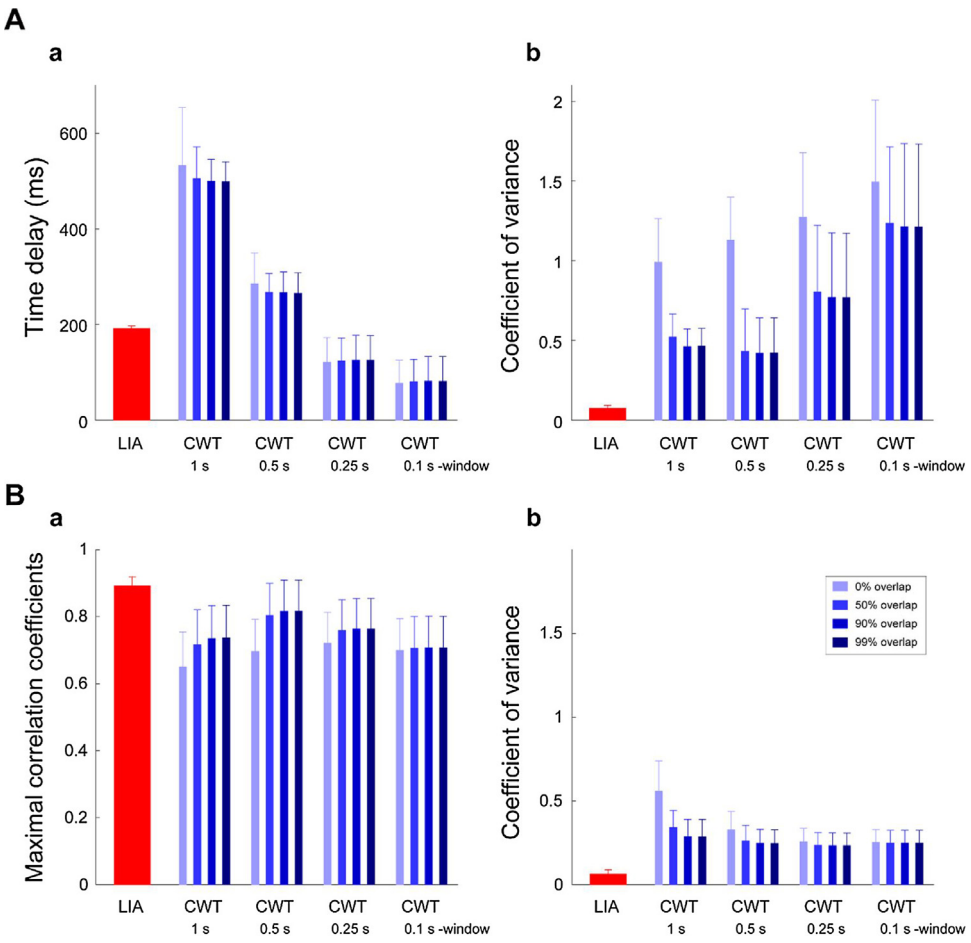

Fig. 6. Comparison of the ERD accuracy and time delay calculated by the online LIA and CWT algorithms in all time windows and overlaps.
A. The average time delay calculated by the online LIA (red bar) and CWT (blue bars) with 1-, 0.5-, 0.25-, and 0.1-s time windows and 0, 50, 90, and 99% overlaps (**a**). The average time delay coefficient of variance calculated by the online LIA (red bar) and CWT (blue bars) with 1-, 0.5-, 0.25-, and 0.1-s time windows and 0, 50, 90, and 99% overlaps (**b**). The error bars represent the standard deviation. **B**. The average MCC calculated by the online LIA (red bar) and CWT (blue bars) with 1-, 0.5-, 0.25-, and 0.1-s time windows and 0, 50, 90, and 99% overlaps (**a**). The average coefficient of variance of the MCC calculated by the online LIA (red bar) and CWT (blue bars) with 1-, 0.5-, 0.25-, and 0.1 s time windows and the 0, 50, 90, and 99% overlaps (**b**). The error bars represent the standard deviation (For interpretation of the references to colour in this figure legend, the reader is referred to the web version of this article.).

the online LIA compared with the CWT ($p < 10^{-5}$; Fig. 6**Cb** and **Cd**) and AR algorithms ($p < 10^{-10}$; Fig. 7**Cb** and **Cd**) for every parameter (also see the beta estimation results in Supplementary Table 2). In summary, these results suggest that the online LIA algorithm has general advantages over the CWT and AR model algorithms in terms of delay, accuracy, and stability, to detect alpha and beta motor-imagery-related SM1-ERDs.

4. Discussion

The present study reports a novel algorithm that can be used in real time to detect amplitude modulation of motor-related alpha ERDs in SM1 using an LIA in healthy participants. We demonstrated the advantages of the online LIA algorithm compared with conventional online FFT, CWT, and AR algorithms as follows. First, the lag time to estimate amplitude modulation of SM1-ERDs using the online LIA was shorter than the commonly used online conventional algorithms (i.e., FFT, CWT, and AR) for most of the parameters; an exception was noted in the shorter time windows of 0.1 s and 0.25 s in the CWT and AR algorithms. Second, the online LIA algorithm estimated SM1-ERDs more accurately than did the online FFT, CWT, and AR algorithms for every parameter of the window length (i.e., 100, 250, 500, and 1000 ms) and overlap (i.e., 0, 50, 90, 99%). Third, the LIA was a more stable algorithm than the online FFT, CWT, and AR algorithms in every parameter, as indicated by the significant decrease in the coefficient of variance of the delay time and MCC across trials by the online LIA algorithm. These results demonstrated that the online LIA algorithm could more instantaneously and stably detect the trends of motor-related SM1-ERDs with a shorter delay than could the conventional FFT algorithm, suggesting that the LIA could be effectively incorporated into the existing BCI paradigms to facilitate neurorehabilitation in patients with motor deficits.

It is well known that the LIA system is a powerful tool for filtering small sinusoidal signals out of random noise by phase-sensitive detection, even in extremely noisy environments (Michels and Curtis, 1941). This algorithm has been utilized in different investigations to detect auditory somatosensory evoked potentials (SSEPs; Euler and Kiessling, 1981) and steady-state visual evoked potentials (SSVEPs; Schacham and Pratt, 1985). This approach using an LIA also succeeded in predicting two different SSVEP signals in a BCI paradigm (McMillan et al., 1995). Similarly, classification accuracy was better using a four-class BCI than with the commonly used discrete Fourier transformation (Müller-Putz et al., 2008). In agreement with these studies showing the effectiveness of an LIA for detecting evoked potentials (e.g., SSEP and SSVEP), we demonstrated incorporation of the online LIA algorithm for use in

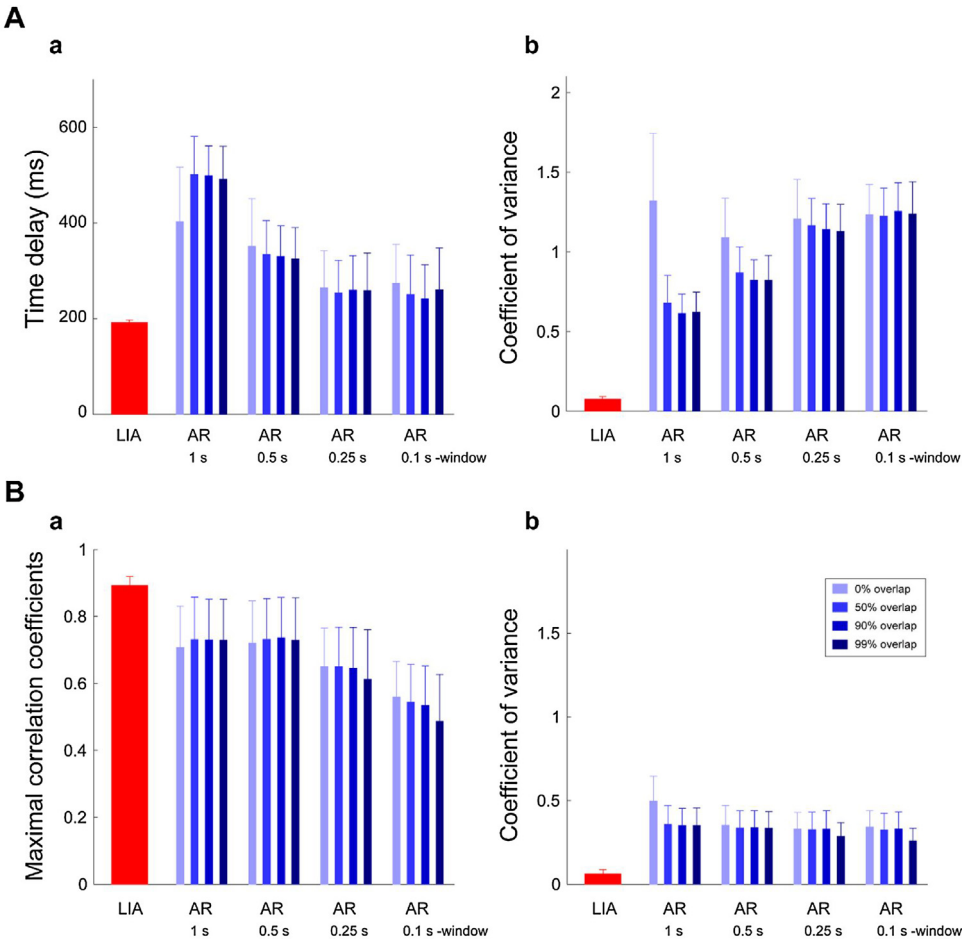

Fig. 7. Comparison of the ERD accuracy and time delay calculated by the online LIA and AR algorithms in all time windows and overlaps.
A. The average time delay calculated by the online LIA (red bar) and AR (blue bars) with 1-, 0.5-, 0.25-, and 0.1-s time windows and 0, 50, 90, and 99% overlaps (**a**). The average time delay coefficient of variance calculated by the online LIA (red bar) and AR (blue bars) with 1-, 0.5-, 0.25-, and 0.1-s time windows and 0, 50, 90, and 99% overlaps (**b**). The error bars represent the standard deviation. **B**. The average MCC calculated by the online LIA (red bar) and AR (blue bars) with 1-, 0.5-, 0.25-, and 0.1 s time windows and 0, 50, 90, and 99% overlaps (**a**). The average coefficient of variance of the MCC calculated by the online LIA (red bar) and AR (blue bars) with 1-, 0.5-, 0.25-, and 0.1-s time windows and the 0, 50, 90, and 99% overlaps (**b**). The error bars represent the standard deviation (For interpretation of the references to colour in this figure legend, the reader is referred to the web version of this article.).

extracting spontaneous amplitude modulation of alpha SM1-ERDs during a motor imagery task in healthy participants.

We found robust improvement in calculating most time windows and overlaps using the LIA compared with the FFT, CWT, and AR algorithms; however, some time delay results calculated by the LIA were longer than or comparable to those found using the AR and CWT algorithms, particularly for the shorter time windows of 0.1 s and 0.25 s (Figs. 6**Aa** and 7**Aa**). Indeed, spectral estimation with the AR model is suggested to be advantageous when short data segments are analyzed, since an analytically derived AR spectrum is infinite and does not depend on the length of analyzed data (Burg, 1972; Al-Fahoum and Al-Fraihat, 2014). Similarly, CWT uses variable-sized windows by scaling the "motor wavelet;" this can provide flexibility in fine time–frequency representation irrespective of the length of data segments (Subasi, 2007). It is also notable that our findings on the stability of MCCs and time delay in the LIA were substantially higher than those found with all conventional algorithms, even with the shorter time windows (Figs. 5**Ab** and 7**Ab**, Supplementary Tables 1 and 2). This result implies that point-by-point calculation by the online LIA algorithm, including simple multiplication of the EEG and reference signal, and integration over one cycle at the FOI may reduce the variance in accuracy and time delay of the ERD estimation, while those calculated by the AR or CWT algorithms may vary depending on the model order selection or mother wavelet type (Al-Fahoum and Al-Fraihat, 2014).

Previous studies have shown that delayed visual feedback attenuates error-based sensorimotor learning during prism adaptation (Kitazawa et al., 1995; Tanaka et al., 2011) and a gradual visuomotor rotation task (Honda et al., 2012). Considering that BCI also requires error-based learning through visual feedback that represents brain activity, such as motor-related SM1-ERDs (Green and Kalaska, 2011; Ono et al., 2013; Hiremath et al., 2015; Ushiba and Soekadar, 2016), appropriate temporal input–output associations might be crucial for BCI learning. Therefore, we believe that the development of an algorithm that enables more accurate and stable estimation of brain activity with a shorter delay would increase control over the BCI in comparison with the conventional online FFT algorithm. Although we demonstrated that the LIA was fast, accurate, and stable for ERD estimation at a single frequency, which revealed the most significant ERD during a motor imagery task, an approach for multi-frequency calculation may be more adaptive and robust for BCI control. Indeed, a previous study showed that the frequency with the highest power at rest fluctuated over time, even within a single participant (Espenhahn et al., 2017). Therefore, future studies should investigate whether multi-frequency calculation via parallel processing of LIAs results in additional improvement in terms of the robustness of ERD estimation.

Finally, previous studies demonstrated that motor-related SM1-ERDs estimated by the conventional FFT algorithm with 500-ms time windows reflected decreased GABAergic intracortical inhi-

bition (Takemi et al., 2013) and spinal motoneuron excitability (Takemi et al., 2015). Further studies should be performed to investigate whether 200 ms faster ERD estimation via the LIA algorithm can assess instantaneous SM1 or spinal excitability more accurately and stably than the conventional FFT-based algorithm.

Competing financial interests

The authors declare no competing financial interests.

Acknowledgments

We thank S. Ishii, K. Nanjo, and S. Ohtaki for their technical support and S. Kasuga for helpful discussion. This study was supported in part by Development Business of Medical Devices/System Study Realizing the Future Medical Care, from Japan Agency for Medical Research and Development (AMED) to J.U., and "Development of Brain-Machine Interface Technology" under the Strategic Research Program for Brain Sciences from AMED to J.U., Keio Institute of Pure and Applied Sciences (KiPAS) research program to J.U., and Grant-in-Aid for Young Scientists (B) and the Ministry of Education, Culture, Sports, Science, and Technology (no. 16K16467) to K.K., and the Sasakawa Scientific Research Grant from the Japan Science Society to K.K.

Appendix A. Supplementary data

Supplementary data associated with this article can be found, in the online version, at https://doi.org/10.1016/j.jneumeth.2017.10.015.

References

Al-Fahoum, A.S., Al-Fraihat, A.A., 2014. Methods of EEG signal features extraction using linear analysis in frequency and time-frequency domains. ISRN Neurosci. 73021, 8, Review.
Ang, K.K., Guan, C., Chua, K.S., Ang, B.T., Kuah, C.W., Wang, C., Phua, K.S., Chin, Z.Y., Zhang, H., 2011. A large clinical study on the ability of stroke patients to use an EEG-based motor imagery brain-computer interface. Clin. EEG Neurosci. 42 (4), 253–258.
Ang, K.K., Chua, K.S., Phua, K.S., Wang, C., Chin, Z.Y., Kuah, C.W., Low, W., Guan, C., 2015. A randomized controlled trial of EEG-based motor imagery brain-computer interface robotic rehabilitation for stroke. Clin. EEG Neurosci. 46 (4), 310–320.
Bos, R., deWaele, S., Broersen, P.M.T., 2002. Autoregressive spectral estimation by application of the burg algorithm to irregularly sampled data. IEEE Trans. Instrum. Meas. 51 (6), 1289–1294.
Broetz, D., Braun, C., Weber, C., Soekadar, S.R., Caria, A., Birbaumer, N., 2010. Combination of brain-computer interface training and goal-directed physical therapy in chronic stroke: a case report. Neurorehabil. Neural Repair 24 (7), 674–679.
Burg, J.P., 1972. The relationship between maximum entropy spectra and maximum likelihood spectra. Geophysics 37, 375–376.
Caria, A., Weber, C., Brötz, D., Ramos, A., Ticini, L.F., Gharabaghi, A., Braun, C., Birbaumer, N., 2011. Chronic stroke recovery after combined BCI training and physiotherapy: a case report. Psychophysiology 48 (4), 578–582.
Claerbout, J.F., 1985. Fundamentals of Geophysical Data Processing with Applications to Petroleum Prospecting. Oxford, UK: Blackwell, pp. 59–62.
Cvetkovic, D., Übeyli, E.D., Cosic, I., 2008. Wavelet transform feature extraction from human PPG, ECG, and EEG signal responses to ELF PEMF exposures: a pilot study. Digit. Signal Process. 18 (5), 861–874.
Daly, J.J., Wolpaw, J.R., 2008. Brain-computer interfaces in neurological rehabilitation. Lancet Neurol. 7 (11), 1032–1043.
Daly, J.J., Cheng, R., Rogers, J., Litinas, K., Hrovat, K., Dohring, M., 2009. Feasibility of a new application of noninvasive Brain Computer Interface (BCI): a case study of training for recovery of volitional motor control after stroke. J. Neurol. Phys. Ther. 33 (4), 203–211.
Espenhahn, S., de Berker, A.O., van Wijk, B.C., Rossiter, H.E., Ward, N.S., 2017. Movement-related beta oscillations show high intra-individual reliability. Neuroimage 15 (147), 175–185.
Euler, M., Kiessling, J., 1981. Frequency-following potentials in man by lock-in technique. Electroencephalogr. Clin. Neurophysiol. 52 (5), 400–404.
Feldman, M., 2011. Hilbert transform in vibration analysis. Mech. Syst. Sig. Process. 25 (3), 735–802.
Ferree, T.C., Luu, P., Russell, G.S., Tucker, D.M., 2001. Scalp electrode impedance, infection risk, and EEG data quality. Clin. Neurophysiol. 112 (3), 536–544.
Ge, S., Wang, R., Yu, D., 2014. Classification of four-class motor imagery employing single-channel electroencephalography. PLoS One 9 (6), e98019.
Green, A.M., Kalaska, J.F., 2011. Learning to move machines with the mind. Trends Neurosci. 34 (2), 61–75, Review.
Gunduz, A., Brunner, P., Daitch, A., Leuthardt, E.C., Ritaccio, A.L., Pesaran, B., Schalk, G., 2012. Decoding covert spatial attention using electrocorticographic (ECoG) signals in humans. Neuroimage 60 (4), 2285–2293.
Hiremath, S.V., Chen, W., Wang, W., Foldes, S., Yang, Y., Tyler-Kabara, E.C., Collinger, J.L., Boninger, M.L., 2015. Brain computer interface learning for systems based on electrocorticography and intracortical microelectrode arrays. Front Integr Neurosci. 9 (40), Review.
Honda, T., Hirashima, M., Nozaki, D., 2012. Adaptation to visual feedback delay influences visuomotor learning. PLoS One 7 (5), e37900.
Hummel, F., Andres, F., Altenmüller, E., Dichgans, J., Gerloff, C., 2002. Inhibitory control of acquired motor programmes in the human brain. Brain 125 (Pt. 2), 404–420.
Kitazawa, S., Kohno, T., Uka, T., 1995. Effects of delayed visual information on the rate and amount of prism adaptation in the human. J. Neurosci. 15, 7644–7652.
Krusienski, D.J., McFarland, D.J., Wolpaw, J.R., 2012. Value of amplitude, phase, and coherence features for a sensorimotor rhythm-based brain-computer interface. Brain Res. Bull. 87 (1), 130–134.
Müller-Putz, G.R., Eder, E., Wriessnegger, S.C., Pfurtscheller, G., 2008. Comparison of DFT and lock-in amplifier features and search for optimal electrode positions in SSVEP-based BCI. J. Neurosci. Methods 168 (1), 174–181.
McMillan, G.R., Calhoun, G.L., Middendorf, M.S., Schnurer, J.H., Ingle, D.F., Nasman, V.T., 1995. Direct brain interface utilizing self-regulation of steady-state visual evoked response (SSVER). Proc. RESNA 18th Annual Conference (RESNA).
Michels, W.C., Curtis, N.L., 1941. A pentode lock-In amplifier of high frequency selectivity. Rev. Sci. Instrum. 12 (9), 444.
Mukaino, M., Ono, T., Shindo, K., Fujiwara, T., Ota, T., Kimura, A., Liu, M., Ushiba, J., 2014. Efficacy of brain-computer interface-driven neuromuscular electrical stimulation for chronic paresis after stroke. J. Rehabil. Med. 46 (4), 378–382.
Ono, T., Kimura, A., Ushiba, J., 2013. Daily training with realistic visual feedback improves reproducibility of event-related desynchronisation following hand motor imagery. Clin. Neurophysiol. 124 (9), 1779–1786.
Ono, T., Shindo, K., Kawashima, K., Ota, N., Ito, M., Ota, T., Mukaino, M., Fujiwara, T., Kimura, A., Liu, M., Ushiba, J., 2014. Brain-computer interface with somatosensory feedback improves functional recovery from severe hemiplegia due to chronic stroke. Front. Neuroeng. 7, 19.
Ono, T., Tomita, Y., Inose, M., Ota, T., Kimura, A., Liu, M., Ushiba, J., 2015. Multimodal sensory feedback associated with motor attempts alters BOLD responses to paralyzed hand movement in chronic stroke patients. Brain Topogr. 28 (2), 340–351.
Prasad, G., Herman, P., Coyle, D., McDonough, S., Crosbie, J., 2010. Applying a brain-computer interface to support motor imagery practice in people with stroke for upper limb recovery: a feasibility study. J. Neuroeng. Rehabil. 7, 60.
Ramos-Murguialday, A., Broetz, D., Rea, M., Läer, L., Yilmaz, O., Brasil, F.L., Liberati, G., Curado, M.R., Garcia-Cossio, E., Vyziotis, A., Cho, W., Agostini, M., Soares, E., Soekadar, S., Caria, A., Cohen, L.G., Birbaumer, N., 2013. Brain-machine interface in chronic stroke rehabilitation: a controlled study. Ann. Neurol. 74 (1), 100–108.
Schacham, S.E., Pratt, H., 1985. Detection and measurement of steady-state evoked potentials in real-time using a lock-in amplifier. Technical note. J. Neurosurg. 62 (6), 935–938.
Schween, R., Hegele, M., 2017. Feedback delay attenuates implicit but facilitates explicit adjustments to a visuomotor rotation. Neurobiol. Learn Mem. 140, 124–133.
Shindo, K., Kawashima, K., Ushiba, J., Ota, N., Ito, M., Ota, T., Kimura, A., Liu, M., 2011. Effects of neurofeedback training with an electroencephalogram-based brain-computer interface for hand paralysis in patients with chronic stroke: a preliminary case series study. J. Rehabil. Med. 43 (10), 951–957.
Subasi, A., 2007. EEG signal classification using wavelet feature extraction and a mixture of expert model. Expert Syst. Appl. 32 (4), 1084–1093.
Takemi, M., Masakado, Y., Liu, M., Ushiba, J., 2013. Event-related desynchronization reflects downregulation of intracortical inhibition in human primary motor cortex. J. Neurophysiol. 110 (5), 1158–1166.
Takemi, M., Masakado, Y., Liu, M., Ushiba, J., 2015. Sensorimotor event-related desynchronization represents the excitability of human spinal motoneurons. Neuroscience 297, 58–67.
Tanaka, H., Homma, K., Imamizu, H., 2011. Physical delay but not subjective delay determines learning rate in prism adaptation. Exp. Brain Res. 208, 257–268.
Ushiba, J., Soekadar, S.R., 2016. Brain-machine interfaces for rehabilitation of poststroke hemiplegia. Prog. Brain Res. 228, 163–183.
Wang, W., Collinger, J.L., Perez, M.A., Tyler-Kabara, E.C., Cohen, L.G., Birbaumer, N., Brose, S.W., Schwartz, A.B., Boninger, M.L., Weber, D.J., 2010. Neural interface technology for rehabilitation: exploiting and promoting neuroplasticity. Phys. Med. Rehabil. Clin. N. Am. 21 (1), 157–178.
Wang, Z., Gunduz, A., Brunner, P., Ritaccio, A.L., Ji, Q., Schalk, G., 2012. Decoding onset and direction of movements using Electrocorticographic (ECoG) signals in humans. Front. Neuroeng. 5, 15.
Wang, Y., Veluvolu, K.C., Lee, M., 2013. Time-frequency analysis of band-limited EEG with BMFLC and Kalman filter for BCI applications. J. Neuroeng. Rehabil. 10, 109.